Construction and Building Materials 223 (2019) 898–909

Contents lists available at ScienceDirect

Construction and Building Materials

journal homepage: www.elsevier.com/locate/conbuildmat

Accounting for steel rebar effect on resistivity profiles in view of reinforced concrete structure survey

Marie Antoinette Alhajj *, Sérgio Palma-Lopes, Géraldine Villain

IFSTTAR, Site de Nantes, 44 344 Bouguenais, France

HIGHLIGHTS

- Reinforcement induces a significant decrease in the apparent resistivity values.
- This effect is sensitive to the concrete cover and the inter-electrode spacing.
- Reinforcement has an effect on the apparent resistivity and not on the 'true' one.
- The methodology developed allows a good modeling of the effects of reinforcement.

ARTICLE INFO

Article history:
Received 18 December 2018
Received in revised form 4 June 2019
Accepted 19 July 2019
Available online 27 July 2019

Keywords:
Steel reinforced concrete
Durability
Non-destructive testing
Electrical resistivity
Numerical modelling

ABSTRACT

Concrete is well known for its durability. However, it is exposed to aggressive agents, such as water and chlorides, leading to its degradation. The DC-electrical resistivity method is a technique devoted to non-destructive evaluation (NDE). However, when applying this measurement technique to reinforced concrete structures, the measurements may be highly influenced by the presence of reinforcement. To study the influence of reinforcements and estimate the impact of their effect on resistivity measurements on concrete, we model their contribution by finite element numerical analysis. Electrical measurements in reinforced and unreinforced concrete slabs were modelled and actual experimental measurements were used. This article presents the numerical study results that are compared to the experimental data for validation purposes. By validating the presented approach, it will be possible to fully account for the effect of the reinforcements, as an alternative to measurement strategies that aim at minimizing the disturbance due to reinforcements.

1. Introduction

Known for its resistance to compression and to tension when reinforced, concrete is also well known for its durability. Despite being a porous material and allowing the penetration of aggressive agents, concrete is capable of resisting to chemical and environmental attacks [1]. Nonetheless, when the amount of intrusive aggressive agents exceeds a certain limit, pathologies appear in the concrete causing its degradation and therefore threaten the service life duration of the structure [2]. For instance, previous studies showed that the critical concentration of chloride ions for corrosion initiation depends on the percentage of cement mass [3]. Furthermore, recent studies have been conducted to measure the critical chloride content [4]. This will permit improving the prediction of the residual service life of a structure. Therefore, we need to determine the concentration of chlorides in the concrete cover in order to predict its residual lifespan.

To evaluate the durability of concrete, the concentration of aggressive agents penetrating through the concrete cover can be evaluated by non-destructive evaluation (NDE) techniques [7]. Measurements made by NDE methods are sensitive to material parameters and allow monitoring the degradations in this material without being intrusive [5]. Among the techniques used to inspect reinforced concrete structures, this study focuses on the DC-electrical resistivity technique, due to its sensitivity to several properties of concrete [6–8]. Electrical resistivity is a bulk physical property that depends on the composition of the material and on its conditioning [9]. On one hand, studies showed that the electrical resistivity of concrete is sensitive to the connectivity and tortuosity of its porosity, and to the water/cement ratio, that also influences porosity [10]. On the other hand, the resistivity depends on the water content as described by Archie's law [11] and it is influenced by the chloride content in concrete [12,13]. Therefore,

* Corresponding author at: 18 Rue Anatole de Monzie, 44200 Nantes, France.
E-mail addresses: marie-antoinette.alhajj@ifsttar.fr (M.A. Alhajj), Sergio.lopes@ifsttar.fr (S. Palma-Lopes), Geraldine.villain@ifsttar.fr (G. Villain).

https://doi.org/10.1016/j.conbuildmat.2019.07.208
0950-0618/

by determining the resistivity of concrete using the DC-resistivity method, one can predict the change in chloride and water contents in concrete. Finally, Rasch and Hinrichsen [14] showed that the temperature has an effect on its resistivity, which means that temperature needs to be taken into account [15]. Due to the sensitivity of the electrical resistivity of concrete to its properties especially to the water and chloride contents, the measurement of resistivity can be associated to durability indicators through calibration [16–18].

By developing the electrical method, it became possible to carry out electrical resistivity tomography (ERT) and determine the resistivity at different investigation depths [19,20]. In this study, we are only interested in one-dimensional (1D) tomography, which leads to the resistivity profile as a function of depth from the surface. Despite having a great benefit in assessing the resistivity of concrete, this ND method is indirect. Using the DC-resistivity method for in situ concrete investigation does not lead to the 'true' resistivity distribution but rather to "apparent" resistivity data. In fact, an apparent resistivity is an integrating value from the concrete surface to a certain depth, which mainly depends on the electrode spacing. Therefore, the process consists of two steps: first, the apparent resistivity measurements then, the inversion of the apparent resistivity dataset. Consequently, the inverted resistivity profiles show the 'true' resistivity distribution in the concrete cover [3,11].

Furthermore, although the DC-resistivity method gives reliable results when applied to inspect the concrete cover layer, measurements are disturbed in the presence of steel reinforcement [21,22,23,24]. The 'apparent' resistivity may significantly decrease due to the high electrical conductivity of steel [25,26,27]. This phenomenon may strongly influence the apparent resistivity measurements, which in turn makes it difficult or even impossible to retrieve the 'true' resistivity of concrete [19].

The evidence of steel rebar effect on apparent resistivity measurements has led to rules of thumb for trying to mitigate such effects. Hence, several approaches have been proposed to minimize the disturbance caused by the reinforcements. A first approach consists of placing the electrodes at a certain distance from the rebars diagonally in the rebar mesh with a preferred spacing for the electrodes between 30 and 50 mm [22,23]. A second approach, based on the method of image charges proposed a mathematical model that takes into account the influence of steel in function of various factors [28]. A third approach is based on creating a model that describes the presence of reinforcement and its short circuit effect by taking the electrochemical state of the steel into account [26,29,30,31]. A fourth approach proposed by Garzon et al. in 2014 [27] and recently by Samson et al. in 2018 [31] consists of introducing a 'rebar factor' in the apparent resistivity formula in order to remove the rebar effect. Both studies were developed for specific slab geometries and for homogeneous concrete with a constant resistivity.

However, in the present study, the aim is to determine the effect of the reinforcement on the resistivity of concrete and to quantify it before the beginning of corrosion, in the initiation period, even when the concrete is non-homogeneous and for a more complex reinforcement mesh in the concrete structure. For this purpose, we use numerical analysis based on the finite element method by creating a model of a concrete slab, adding a steel bar to it and then simulating electrical measurements. In that sense, our study shares some common methodology with that of Presuel-Moreno et al. [32]. In fact, both studies deal with determining the effect of steel in function of geometric properties related to the position of the electrodes and the rebar. In addition, the present article deals with a real case study where experimental measurements on a reinforced concrete structure were modeled, in a more complex framework concerning the rebar and the concrete resistivity. Therefore, comparable results as well as new results will be mentioned explicitly.

The aim of this article being the study of the effect of steel reinforcement on the determination of the resistivity distribution in concrete, this effect is firstly observed on the measurements, thereby on the "apparent" resistivity measurements. Hence, the effect must be studied on the measurements at first. Using numerical analysis, we will study the forward problem that consists of simulating apparent resistivity measurements on reinforced concrete and then, the comparison between the measured and the simulated apparent resistivities leads us to determine the effect of the steel reinforcement on the determination of the resistivity of concrete. To this purpose, several models are created to conduct a parametric study of the effect of reinforcement in terms of geometric properties related to the positioning of the measuring device near the reinforcement, and in terms of other properties related to the conditioning of concrete. Then the results are used to model the measurements done on a slab with a more complex rebar mesh, which will lead to many deductions and perspectives for the research.

The hypotheses adopted to carry out this study are briefly stated in the following. Firstly, it is assumed that the presence of rebars in the concrete does not modify the state of the concrete that is near the rebars, at least before corrosion is initiated. Secondly, although polarization may occur at the steel-concrete interface in reinforced concrete [27], the present work aims at investigating the contribution of the purely conductive (non-polarizing) component. Hence, it is assumed here that a steel rebar acts as an extremely conductive body in perfect electrical contact with the concrete. Hence, and no electro-chemical or polarization phenomena are taken into account at the steel-concrete interface.

Thirdly, we assume that the finite element method is capable of simulating the effect of a conductor with limited dimensions, extreme resistivity contrast with the surrounding material, and a certain proximity to the electrodes. Finally, in our study we are only interested in the distribution of resistivity in concrete with depth.

2. DC-electrical resistivity measurement method

In this section, the measurement principle is recalled and the measurement method used in this study is presented.

2.1. Electrical resistivity of concrete

2.1.1. Basic theory

The electrical resistivity of a material, noted ρ, is the ability of this material to oppose the flow of free electric charges when it is subjected to an electric field.

Ohm's law expresses that the current density vector is directly proportional to the electric field by using the electrical conductivity, σ (reciprocal of resistivityρ), as the proportionality factor:

$$\vec{J} = \sigma \vec{E} \tag{1}$$

$\vec{J}$: current density (A/m^2),

$\vec{E}$: electric field (V/m).

In electrostatics, Poisson's equation is given by Eq. (2) and consists of finding the electric potential scalar field V for a given resistivity distribution and charge distribution Q:

$$\nabla.(1/\rho \nabla V) = Q \tag{2}$$

Eq. (2) is used to calculate the forward problem response, i.e. the potential difference due to the injection of a direct current, for a certain spatial resistivity distribution.

2.1.2. Measurement principle

The resistivity ρ of a homogenous and semi-finite medium is an Ohm's-law ratio of measured voltage V to applied current I, multiplied by a geometric constant G [33]:

$$\rho = V/IG \tag{3}$$

where G is the geometric factor that depends on the size and shape of the sample as well as the inter-electrode spacing in the rest of the article [34]. The calculation method of G is developed in Section 2.2.

However, concrete is neither a homogeneous nor a semi-finite medium, therefore the measured resistivity is not the 'true' resistivity and it is called an apparent resistivity ρ_a [35].

As mentioned previously, the electrical resistivity of concrete depends on several properties related to its components, its formulation and its environment. Hence, many factors will influence the resistivity in an uncontrolled environment leading to difficulties in isolating the effect of the reinforcement. Therefore, the concrete studied in this paper and presented in Section 4 is considered homogeneous regarding the aggregates used, the temperature and the water or chloride content, by means of calibration.

The resistivity of concrete can be estimated by the DC-resistivity method that consists of using sets of electrodes with different configurations. Studies have shown that using four electrodes, two for injection and two other ones for the potential drop measurement, is recommended to overcome the problem of contact resistance when using only two electrodes [36,37]. In this study, we will focus on the Wenner alpha configuration (simply called Wenner throughout this paper), characterized by four electrodes equally spaced by a distance "a", where the two external electrodes are used to inject the current and the internal ones are used to measure the potential drop (Fig. 1) [38]. Studies have shown that this configuration has a significant signal to noise ratio. Furthermore, it was used in previous research for the study of steel effect on the resistivity measurements [27,32].

2.2. Resistivity measurement device

One-dimensional electrical resistivity tomography (1D ERT) is a method used in this study to determine the resistivity distribution with depth in concrete by making measurements on the surface, using different spacings between electrodes [20]. ERT data are collected with an automated multi-electrode resistivity meter. This technique was used to develop a multi-electrode resistivity probe by du Plooy et al. (2013) [39] (Fig. 1) using the Wenner configuration presented in the previous section. The multi-electrode resistivity probe consists of 14 electrodes that are equally spaced at a 20 mm interval. Therefore, for all possible Wenner combinations, 26 surface measurements are possible with four different electrode spacings: 20 mm, 40 mm, 60 mm and 80 mm. In this study, the probe was connected to a Syscal Pro® (IRIS Instruments) commercial resistivity meter that generates current transmissions and records the potential drops for all selected 4-electrode combinations. The results obtained represent the "apparent" resistivity data measurement on concrete for four investigation depths. For the first investigation depth, corresponding to the spacing a = 20 mm between the electrodes, 11 measurements are possible. Then this number decreases to 8 measurements for the second spacing (a = 40 mm), then 5 measurements for the third spacing (a = 60 mm) and finally 2 measurements for the largest possible electrode spacing (a = 80 mm). As the concrete specimens are not semi-infinite and to avoid border effects, the geometric factors used are calculated by numerical modelling using the finite element software, COMSOL Multiphysics® in order to take into consideration the geometry of the structure and the position of the electrodes [39,40]. The calculation method consists of simulating a concrete model with the same dimensions and electrode position than the concrete block used for the measurement and with known homogeneous resistivity ρ_0. Then after calculating the potential difference ΔV_0 for this model, the geometric factor is given by:

$$G = \frac{\rho_0 \times I}{\Delta V_0} \tag{4}$$

As stated before, the electrical method using the resistivity probe (Fig. 1) produces "apparent" resistivity values ρ_{a_i} for four electrode spacings (i = 1–4). Therefore, an inversion process needs to be performed in order to reconstruct the 'true' resistivity distribution [41].

2.3. Influence of steel reinforcement

Being a highly conductive material compared to concrete (by 7–9 orders of magnitude, [42]), the steel reinforcements can significantly disturb the electrical current flow [23] and a significant decrease in the measured apparent resistivity can be observed. Numerical studies by Presuel-Moreno et al. [32] and Garzon et al. [27] confirmed that the effect of rebar in a concrete structure was significant and could lead to lower apparent resistivity measurement readings. This effect was also studied by changing some factors like the concrete cover and the position of the electrodes, which will be discussed in this study as well.

3. Numerical simulation

The influence of the reinforcement on the apparent resistivity measurements depends on several parameters related to the position of the measurement device in relation to the steel rebar [44]. Therefore, a parametric study is necessary to take some of these parameters into account. Firstly, we study the thickness of the concrete cover. Secondly, we examine the lateral distance between the axis of the resistivity probe and the axis of the reinforcement, the two axes being parallel. Finally, we consider the orientation of the resistivity probe with respect to the axis of the reinforcement bar.

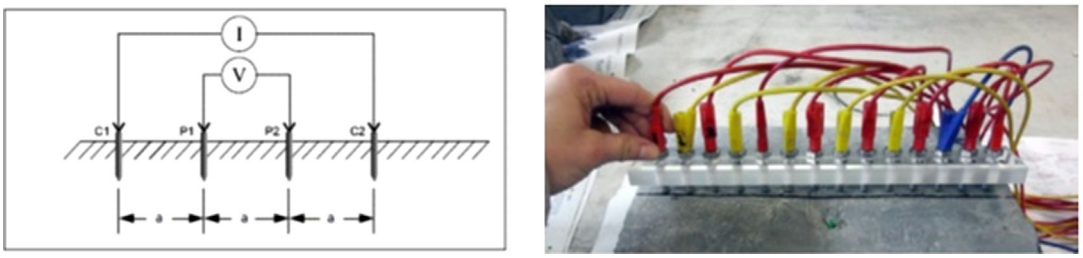

Fig. 1. The Wenner configuration with inter-electrode spacing "a" – 1b a 14-electrode resistivity probe for ERT measurements [39].

3.1. Characteristics of the reference model

A first model of the concrete slab was created. This model was taken as a reference for the others. Then another model of the same concrete slab to which was added one steel bar was studied. It served to determine the influence of the reinforcement on the apparent resistivity regarding geometric properties related to the position of the electrodes near the reinforcement. The modeling was carried out with a commercial finite element analysis software package COMSOL ® Multiphysics, V 5.3 using the module AC/DC.

The physical problem is expressed by the equations presented in Section 2. Punctual electrodes placed on the surface of the slab serve to inject the current. The slab is isolated from the surrounding environment. The reference model is a $900 \times 700 \times 150$ mm^3 homogeneous concrete slab of predefined resistivity of 100 Ω·m. The chosen dimensions refer to those of the slabs used for in situ NDE testing during the experimental campaign presented in Section 4. Then the four-electrode array is placed at the center surface of the upper surface of the slab such as the spacing between two electrodes is 20, 40, 60 and 80 mm. A direct current of intensity equal to 1 A is injected into the model through the external electrodes. Using Eq. (3), the apparent resistivity ρ_a is calculated for each spacing "a". As previously mentioned, the concrete in this model is considered homogeneous having a constant resistivity of 100 Ω·m. Thereby, the apparent resistivity for each spacing should theoretically be equal to 100 Ω·m, as a consequence of the apparent resistivity definition.

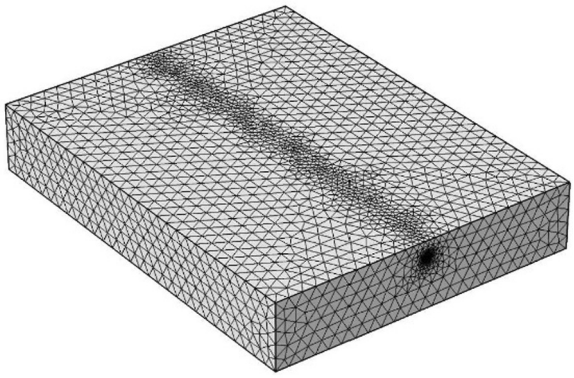

Fig. 2. Meshed model of the 900 × 700 × 150 mm3 concrete slab with a reinforcement of Ø=12 mm at 30 mm depth and a spacing of 80 mm between the electrodes.

The second model is built from the reference model. A steel cylinder of resistivity equal to 0.25×10^{-6} Ω·m representing the reinforcement of diameter Ø=12 mm and of length equal to the concrete slab length (900 mm), is placed on the centerline of the slab and at a depth of 30 mm from the concrete surface. The electrodes are aligned right above the cylinder axis and parallel to it (Fig. 2). The apparent resistivity is also calculated for the model with the steel cylinder.

Comparing the apparent resistivity for the two models (Fig. 3), we can notice that the apparent resistivity values simulated in the reinforced slab are lower than those in the unreinforced one, for each spacing. In addition, the more the spacing increases, the more the investigation depth increases and becomes comparable to the cover thickness. Therefore, the simulated measurement is more and more sensitive to the presence of the very conductive steel bar.

Although an analytical solution was published for expressing the surface electrical potential distribution in the presence of an embedded cylinder of high conductivity [25,43], it only applies to infinitely long cylinders in a semi-infinite medium. Moreover, it assumes that the cylinder radius is significantly smaller than other dimensions (e.g. concrete cover thickness). Therefore, no reference solution is available for validating our numerical solutions. Our results were validated by means of three approaches. In the first approach (not presented here), we checked the convergence of the numerical solutions with respect to the refinement of the finite element meshes used in this study. In the second approach, we compared the solution for the single rebar model (Fig. 2) to a similar model in which the steel cylinder is substituted by a hollow cylinder of which the surface is set to a 'ground' boundary condition (i.e. equivalent to a short-circuit). The latter model yielded identical results to the model with the steel cylinder (Fig. 3). This original approach allowed showing that the modelling method used in the present study as well as in [32], i.e. modelling a rebar as a cylinder of extremely high electrical conductivity having a perfect contact with the concrete, is simply equivalent to setting a short-circuit at the concrete/cylinder interface. The last approach, presented in Section 4, consisted of numerically modeling an experimental case to compare the numerical results with real data acquired on concrete samples.

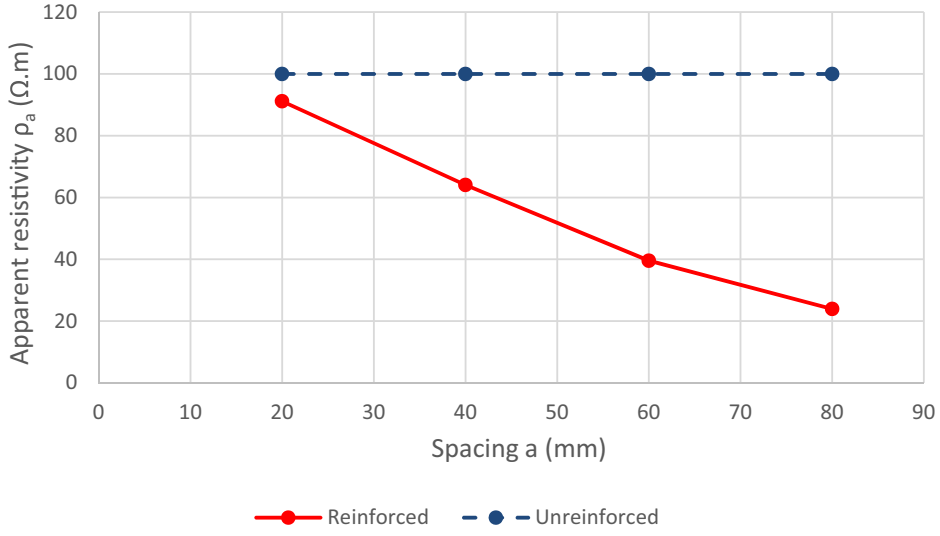

Fig. 3. Comparison of simulated apparent resistivity values vs. electrode spacing between a (single rebar) reinforced and an unreinforced slab.

In the next section, the effect of reinforcement is studied regarding geometric parameters related to the position of the electrodes relative to the reinforcement.

3.2. Parametric study

The purpose of this parametric study is to numerically quantify the effect of the reinforcement on apparent resistivity measurements over the concrete slab. Four parameters are studied on the model of the concrete slab with one single reinforcement bar (Fig. 4):

- the concrete cover thickness h,
- the lateral distance between the electrode line and the rebar axis Δx,
- the orientation of the electrode line relative to the rebar axis in the plane (angle θ),
- and the concrete resistivity.

3.2.1. Concrete cover thickness

The first parameter studied is the concrete cover thickness, h. In this parametric study, the concrete cover thickness h varies from 20 mm, which is the minimum value for a reinforced concrete structure, to 50 mm, which is the thickness of the concrete cover used in structures built in seawater.

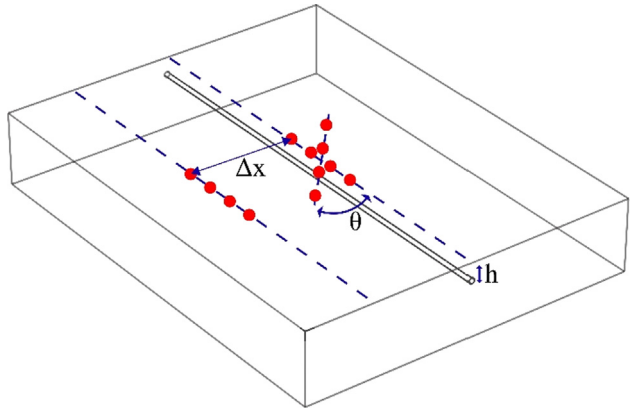

Fig. 4. Modeled reinforced slab showing the geometric parameters for the parametric study.

We recall that the simulated concrete has a resistivity of 100 Ω·m. In the absence of reinforcement, it would be expected to obtain apparent resistivities very close to this value. All the curves presented in Fig. 5 have the same tendency: for each concrete cover thickness, the apparent resistivity decreases as a function of the inter-electrode spacing. Comparing all the curves for a given spacing value, it should be noted that the greater the concrete cover thickness, the lower the effect of the reinforcement on apparent resistivity. This effect was also observed on the results held by a previous numerical study [32].

3.2.2. Lateral distance between the electrode line and the rebar axis

The electrodes are aligned parallel to the axis of the reinforcement. Δx denotes the distance of the line of electrodes perpendicular to the projection at the surface of the axis of the rebar (Fig. 4). In this study, the electrode line is moved respectively by $\Delta x = 40$, 80, and 120 mm from its initial position to evaluate the sensitivity of the apparent resistivity to this distance. The concrete cover thickness is fixed at 30 mm.

Fig. 6 shows the apparent resistivity curves as a function of the inter-electrode spacing for each value selected value of distance Δx. They all exhibit a decreasing behavior with spacing a, which confirms that the effect of the reinforcement is always present even by moving the electrodes laterally with respect to the reinforcement (Fig. 6), which can be also confirmed by the study of Presuel-Moreno et al. [32]. However, this decay is not identical for all distances Δx. In fact, the further the electrode line is from the axis of the reinforcement, the slower the apparent resistivity decreases with the inter-electrode spacing. Thus, for a spacing of 20 mm, it is preferable to move the electrode line by at least 40 mm to reduce the effect of the reinforcements to less than 2% for h = 30 mm. While for a spacing of 40 mm, it is preferable to move the electrode line 80 mm away from the axis of the rebar so that the effect is less than 5%, for h = 30 mm. The spacing a = 40 mm is about the classical spacing used for commercial Wenner resistivity devices. As a rule of thumb, one can keep in mind that for a Wenner array the lateral distance between the

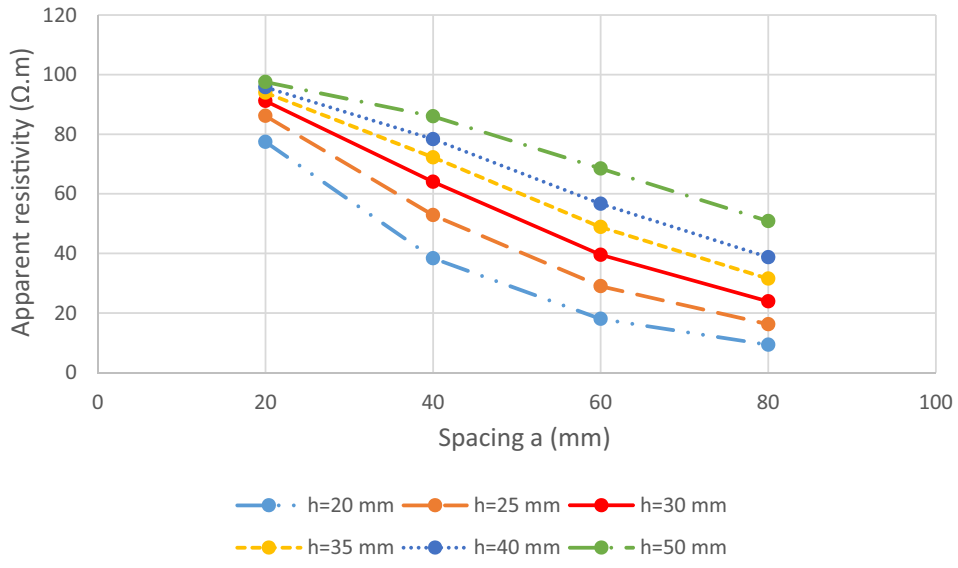

Fig. 5. Simulated apparent resistivity vs. electrode spacing for different concrete cover thicknesses.

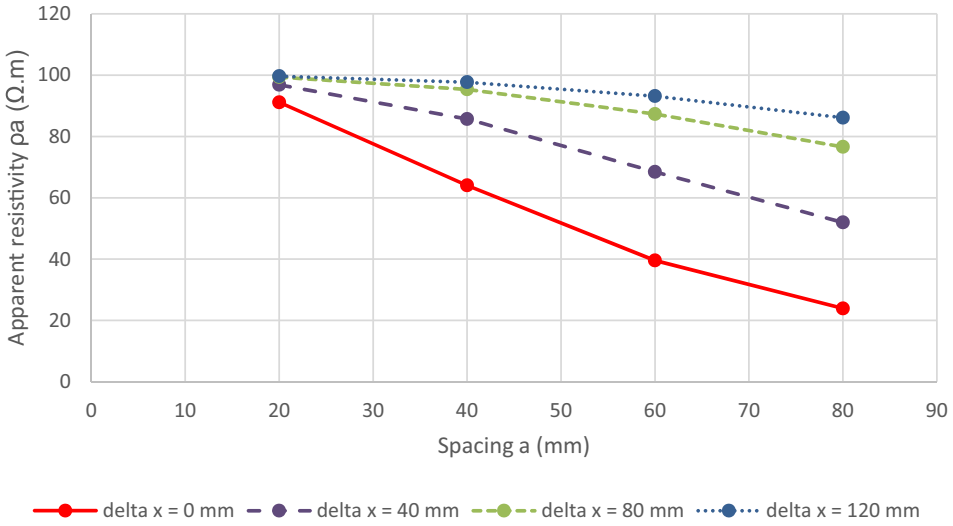

Fig. 6. Simulated apparent resistivity with respect to the electrode spacing for different lateral distances x of the electrode line on the concrete surface (h = 30 mm).

four-electrode line and the closest rebar axis should be at least twice the inter-electrode spacing.

3.2.3. Orientation of the electrode line

The electrodes are initially aligned directly above the reinforcement axis such as the electrode line is parallel to the reinforcement axis. In this section, the angle θ between the center of the electrode line and the rebar axis varies from 0° to 90° (Fig. 4).

Fig. 7 shows the variation of the apparent resistivity as a function of the spacing a for various values of angle θ. Comparing the results, all the curves have approximately the same tendency: the apparent resistivity decreases when the inter-electrode spacing increases. However, it is noticed that the more the angle θ increases, the more the electrode line is deviated from the reinforcement axis and thus the less the effect of the reinforcement is noticeable. Indeed, when the electrode line is perpendicular to the reinforcement axis, the apparent resistivity hardly varies and is almost the same as the reference apparent resistivity. These results agree with the numerical study by Presuel-Moreno et al. [32].

3.2.4. Resistivity of the concrete slab

It is necessary to study the effect of the contrast of resistivity between concrete and steel. For this study, different values of resistivity for the concrete chosen to model the slab are imposed, while maintaining the resistivity of the steel rebar at a fixed value of about 0.25×10^{-6} Ω·m. These values are the classical concrete resistivites and are 20, 100, 1000 and 2000 Ω·m [12]. Each of these values is considered as a reference in the corresponding modelling. Indeed, as previously stated, the resistivity value assigned to a modelled concrete slab is considered as the reference apparent resistivity, as it represents the value that should theoretically be measured on a non-reinforced concrete slab.

The simulation results obtained are shown in Fig. 9. In terms of relative difference between the simulated and the reference apparent resistivity, it can be noticed that for the four curves, the relative difference increases from about 10% for a = 20 mm to about 75% for a = 80 mm. This means that the effect of the reinforcement is almost the same regardless of the resistivity of the concrete, as if the resistivity of steel which is about 10^{-6} Ω.m was so low compared to that of concrete that it is considered as "perfect

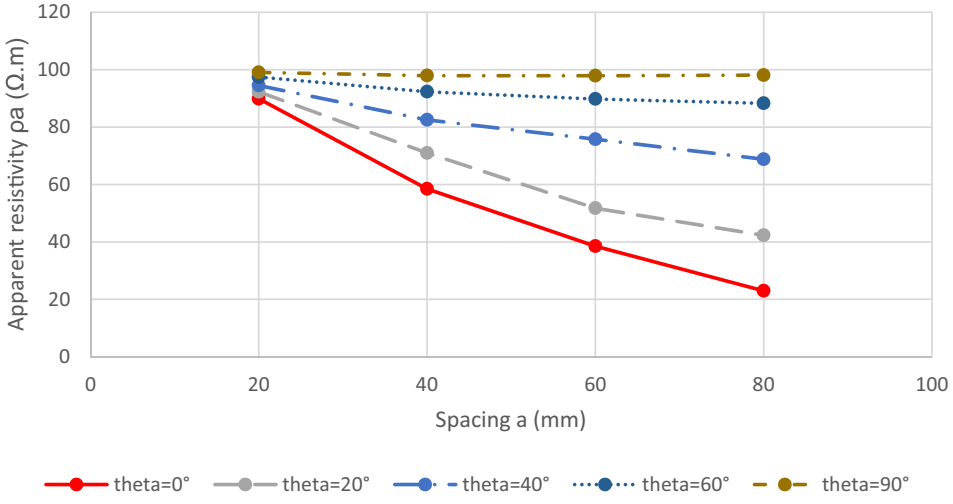

Fig. 7. Simulated apparent resistivity with respect to the electrode spacing for different orientations of the electrode line with respect to the axis of the reinforcement (h = 30 mm and Δx = 0).

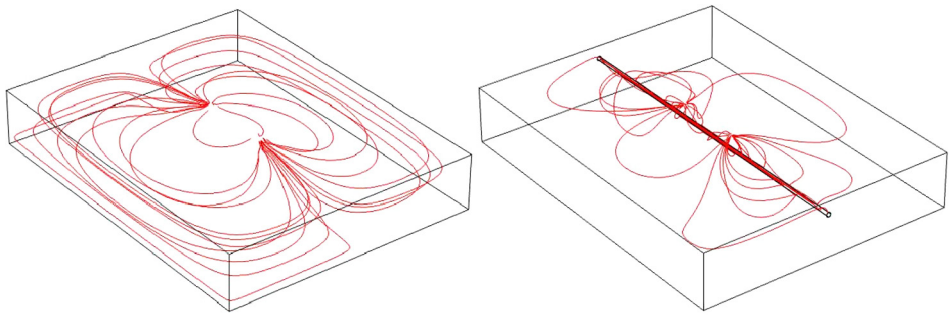

Fig. 8. Current lines in the 3D concrete slab model a- without rebar b- with one steel bar of diameter 12 mm at 30 mm from concrete surface.

conductor", always bringing the same effect of a "perfect short circuit". This is also clear in Fig. 8 where the current lines are disturbed and converge in the steel bar.

This parametric study shows that the apparent resistivity is highly disturbed by the reinforcement that causes a short circuit effect due to the extremely high resistivity contrast between concrete and steel. However, this effect depends on h, Δx and θ. In the next section, the effect of the reinforcement is studied on measurements carried out during an experimental campaign.

4. Application to experimental data

In the previous section, we presented a parametric study using our numerical modelling for estimating rebar effects on DC-electrical measurements. The aim of this section of the paper is to present the application of this procedure to existing experimental data both for testing and for validating it.

The effects of steel reinforcement on the apparent electrical resistivity using the Wenner probe technique were studied experimentally on reinforced concrete slabs that were designed in labs or found in field. Many investigation parameters related to the rebars were studied: the concrete cover thickness [44,45], the complexity of the rebar mesh, the probe configuration, the rebar coating [44]. However, studies showed that there are many other challenges for real-time resistivity measurements. For instance, temperature could have a non-negligible effect on resistivity measurements in the real and uncontrolled environment [46]. Therefore, temperature effect should be estimated and corrections should be applied [47,48]. In addition to that, the saturation conditions of concrete have a major effect on the resistivity measurement [45,46]. On one hand, the reliability of resistivity measurements on field concrete structures depends on the time for concrete to reach a certain saturation ratio and for the resistivity measurements to stabilize [46]. On the other hand, with environmental conditions like rain a more complex situation is observed in which reinforced concrete is subjected to wet/dry cycles of different duration. Under those conditions, it becomes more difficult to estimate the resistivity gradient in concrete [45]. In our study, we assume that the concrete slabs designed for lab measurements are kept in controlled conditions, i.e. constant temperature and salt water imbibition level during the 2-day duration of the imbibition process (Section 4.1). Under these conditions, we will assume a simple resistivity profile in the concrete slabs (Section 4.3).

4.1. Formulation of concretes and preconditioning of test specimens

The APOS French research project consisted of non-destructive evaluation on concrete slabs in order to assess the durability of reinforced concrete structures and the evolution of the deteriorations in time. The focus of the study is on degradations of reinforced concrete structures in the marine environment. The non-destructive measurements are made on slabs of dimensions $900 \times 700 \times 150\ mm^3$. Some are reinforced and others are not. For reinforced slabs, the concrete cover is characterized by a nominal thickness of 30 mm. The steel rebars used are classic high adherence HA12 bars of diameter 12 mm and are arranged to obtain four meshes of dimensions $200 \times 300\ mm^2$ (Fig. 10). The slabs studied are made of cement type C25/30 mixed with CEMI Portland cement and are designated C1. The water to cement ratio is 0.6. Table 1 summarizes the composition of concrete C1. The compressive strength at 28 days is 36.3 MPa with a standard deviation of 0.86 and the porosity at 28 days is 15.6% with a standard deviation of 1.5. A set of 10 slabs was manufactured for different types of non-destructive tests. Then, pre-conditioning of the slabs was performed with the aim to obtain homogeneous slabs at time T_0 that is the starting point of the subsequent imbibition phase. An imbibition of the slabs in 10 mm of salt water at a concentration [NaCl] = 35 g/L was performed for more than one year. Measurement campaigns took place at seven times and this study focuses on the first four times: $T_1 = T_0$+1h, $T_2 = T_0$+4h, $T_3 = T_0$+18 h and $T_4 = T_0$ + 38 h. At each test time, the slabs were removed from the salt water and flipped over so that the measurements could be performed on the humid face. Then, the slabs were put again in the pool containing salt water.

4.2. Presentation of measurements

In this section, we are interested in the measurements made on the slabs designated by "C1-13" and "C1-14". The C1 refers to the cement type CEMI used and the numbers 13 and 14 refer to the slab number between the remaining specimens. The first slab (C1-13) is unreinforced and subjected to imbibition in salt water and the second (C1-14) contains the meshes of reinforcement described previously and is subjected to imbibition in salt water. Measurement were made using a SYSCAL Pro resistivity meter (IRIS Instruments) that allows to significantly mitigate polarization issues by transmitting a low frequency (2 Hz) alternating square-shaped current and by applying some signal processing to remove any voltage due to remaining polarization. Moreover, the number of cycles of the transmitted signal for one particular measurement (between 3 and 5 cycles) as well as the current intensity (about 1 mA) are usually kept low in order to avoid unnecessary electrode or rebar polarization.

Apparent resistivities were measured with the 14-electrode resistivity probe described in Section 2. In Fig. 10, the electrodes are represented by 14 blue squares on the block surface and aligned on the diagonal of the rectangle formed by cylindrical rebars A, B, 2 and 3. Three measurements were made on the mesh AB23 (Fig. 10): two measurements on the first diagonal of the mesh and one measurement on the cross diagonal by placing the resistivity probe in central position to avoid the effect of the steel

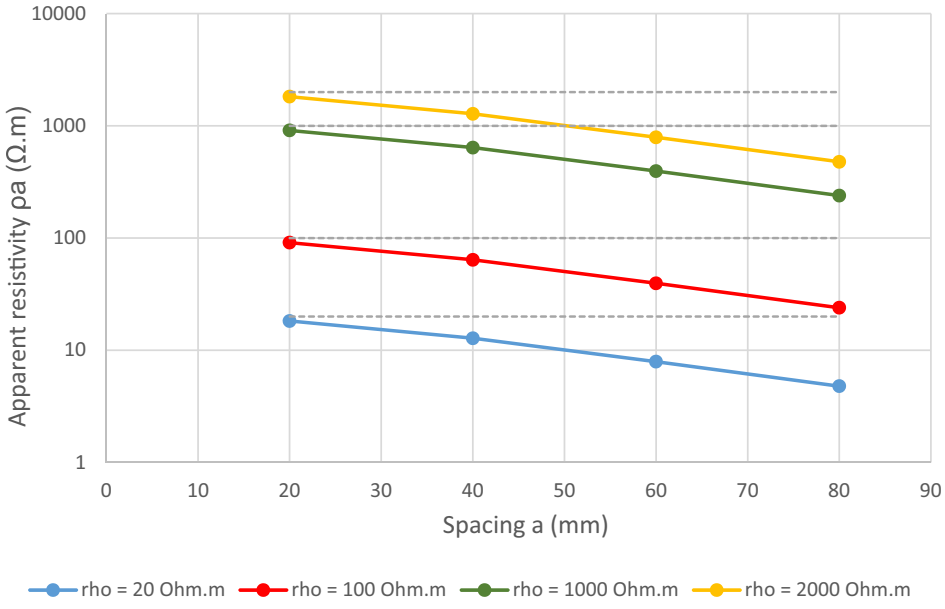

Fig. 9. Apparent resistivity difference between the simulated and the reference apparent resistivity as a function of the spacing between electrodes for different resistivities of the concrete slab (for h = 30 mm and Δx = 0 mm).

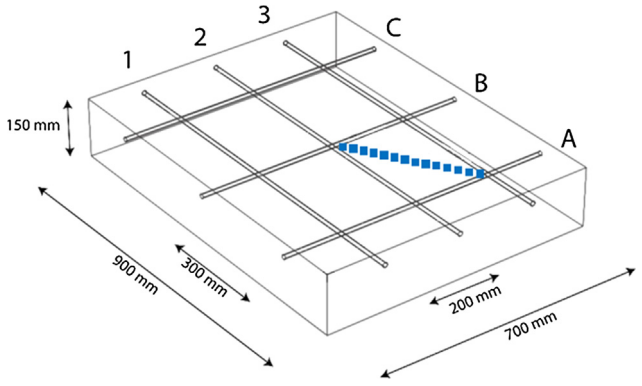

Fig. 10. Geometry of the synthetic model of the reinforced slab (concrete cover thickness is 30 mm; perpendicular rebars are located at the same depth and therefore interpenetrate each other in the model).

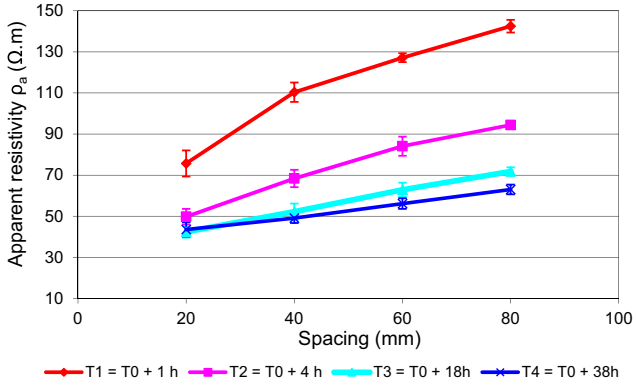

Fig. 11. Experimental apparent resistivity measured on the unreinforced slab C1-13 as a function of inter-electrode spacing at four various test times.

Table 1
Composition of concrete C1 for the experimental campaign.

Component		Source	Quantity (kg, L)
Aggregate 1	11.2/22.4	Quarry of Pont de Pierre (22)	760
Aggregate 2	6.3/10	Quarry of Trègueux (22)	320
Sand 1	0/2	Quarry of Gouviard (22)	56
Sand 2	0/4	Quarry of Moulin (56)	300
Cement	CEMI	Saint-Pierre La Cour	305
Admixtures	AD	Sika Prise SC2	0.7
Water			190

bars as much as possible. On slab C1-13, even if there are no reinforcements, the resistivity measurements were made at the same positions. To obtain the apparent resistivity, the measured transfer resistances (V/I) were then multiplied by the corresponding geometric factors G, modeled using the finite element method described previously in Section 2.2. The mean value and standard deviation of all three measurements were calculated for each slab.

In Fig. 11, the apparent resistivities obtained on the unreinforced slab are shown for all times. The apparent resistivity decreases over time starting with the outer surface in contact with salted water. In fact, the more the quantity of penetrating water increases, the more the resistivity decreases, which is amplified by the presence of chloride ions. In addition to that, for each time, the apparent resistivity increases with the spacing between electrodes, hence with depth due to decrease of moisture and ionic content in concrete with depth. By inverting these curves using the Res1D software [49], we obtain the curves showing the 'true' resistivity distribution of concrete as a function of depth as shown in Fig. 12. The effect of the water penetration from the outer surface is well observed.

Fig. 13 shows the apparent resistivities of the reinforced slab C1-14 for all periods T1–T4. As shown in this figure, the curves do not exhibit a monotonic increase as in the case of the unreinforced slab (Fig. 11). Resistivities decrease from the spacing of 60 mm as the investigated volume increases to include the reinforcement, which agrees with the results of our parametric numerical studies. Therefore, the inversion of apparent resistivities for slab C1-14 by Res1D software is made impossible, which means that, because of the significant disturbance due to the reinforcement, the apparent resistivity datasets are not compatible with a

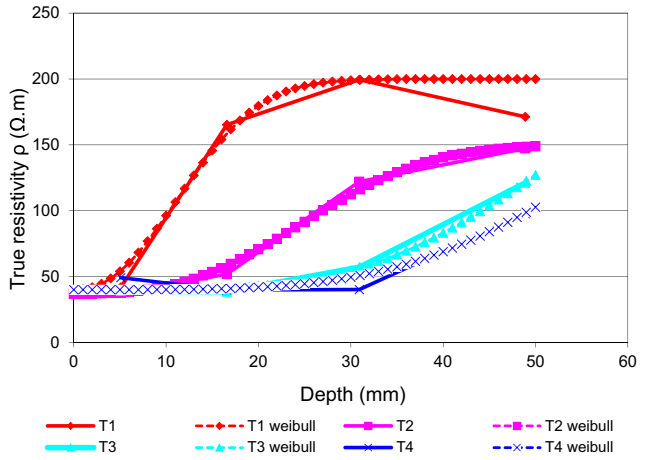

Fig. 12. True resistivity profiles at four test times (slab C1-13) obtained by inversion using Res1D and fitting with Weibull curves.

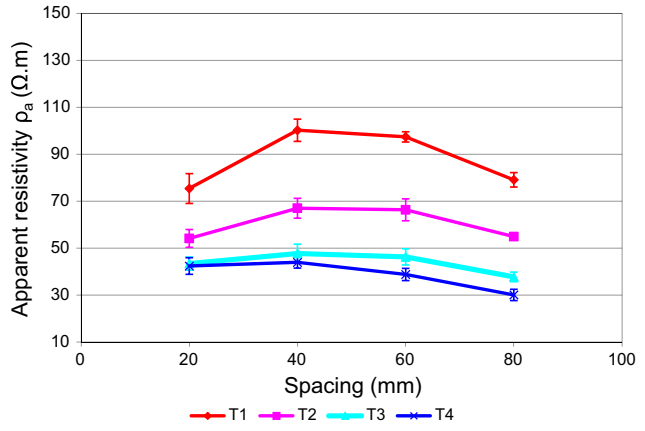

Fig. 13. Experimental apparent resistivity measured on the reinforced slab C1-14 as a function of inter-electrode spacing at four various test times.

1D-resistivity distribution anymore. The significant disturbance due to reinforcement has to be modelled in a forward FE modelling prior to the inversion.

4.3. Inverted resistivity profiles in concrete

For the numerical modeling, it is necessary to be able to assign to the synthetic slab a resistivity profile similar to that of the actual slab. Therefore, the measured apparent resistivites are inverted using Res1D software into a multilayer distribution of the 'true' resistivity (Fig. 11). Then, these 'true' resistivities obtained by inversion can be adjusted to obtain continuous profiles that can be used as input parameters in the modeling. Each resistivity distribution (T1–T4) for the slab C1-13 is fitted by a 4-parameter Weibull distribution as shown in Fig. 12, referring to Fares et al. [50] in order to obtain smooth resistivity profiles. The Weibull distribution is of the form:

$$\rho(z) = (\rho_{min} - \rho_{max}) \times exp(-(z/\lambda)^k) + \rho_{max} \quad (5)$$

where ρ_{min} is the minimum resistivity in the concrete slab (Ω.m),
ρ_{max} the maximum resistivity in the concrete slab (Ω.m),
λ and k the parameters of the Weibull distribution,
with z being the coordinate perpendicular to the slab surface (mm).

4.4. Description of numerical models

The goal here is to verify that a stable solution to the previously defined forward problem can be obtained for a more realistic model of unreinforced or reinforced concrete slabs and to compare the simulated apparent resistivity values with those obtained experimentally on the real slabs. The studied slabs were subjected to water and chloride ingress for the purpose of generating a resistivity gradient that evolves over time.

To solve the forward problem for simulating the measured apparent resistivity values, it is necessary to first estimate the 'true' resistivity profiles as a function of depth in the material, for each test time, and use it as an input for the synthetic model the slab. Thus, for the unreinforced slab, the Weibull curves adjusted and presented in Fig. 12 are used to impose corresponding concrete resistivity profiles to the corresponding synthetic slab.

For the reinforced slab, we assume that the 'true' resistivity profiles of concrete are identical for both unreinforced and reinforced slabs. Since both slabs (C1-13 and C1-14) have indeed the same concrete formulation, both underwent the same imbibition protocol and drying conditions, it is assumed that the condition of the concrete is the same in both slabs. As a result, the 'true' resistivity profiles retrieved in the form of Weibull distributions for the unreinforced slab are applied to the reinforced slab model as well.

So the reinforced slab model consists of two components:

i) the concrete itself to which we impose the same resistivity profiles as those for the unreinforced slab at the respective test times and
ii) the reinforcement represented by six steel cylinders of 12 mm diameter and located under a concrete cover thickness of 30 mm (Fig. 10). It should be noted that in the synthetic slab, the cylinders interpenetrate each other, whereas in the real slab they are placed one above the other, which can cause differences between measured and simulated values for the reinforced slab. Nevertheless, the rebars modeled in this case are much more realistic, and numerically complex, than the one bar case studied in Section 3.

The same positions of the electrodes (on the diagonal of rectangle AB23 formed by cylinder axes A, B, 2 and 3) are set for both the unreinforced and the reinforced slabs. Then, based on the numerical procedure presented in this paper, we predict the apparent resistivity values that would be expected on the experimental slabs having the above-mentioned resistivity profiles. The computation time ranges from a few seconds for the unreinforced slab to about 5 min for the reinforced one, for each four-electrode array.

4.5. Numerical results and comparison to the experimental data

In this section, the numerical and the experimental apparent resistivity values are compared both with graphs and by calculating an overall RMSE (root-mean-square error) according to the following expression:

$$RMSE = \sqrt{\frac{\sum_{i=1}^{4}\left(\rho^i_{a\_expe} - \rho^i_{a\_num}\right)^2}{4}} \quad (6)$$

where $\rho^i_{a\_expe}$ and $\rho^i_{a\_num}$ are the average apparent resistivity measured on the real slab and the average apparent resistivity modeled on the synthetic slab for investigation depth "i" respectively. The graphs showing the experimental and the simulated apparent resistivity values at each test time are presented in Fig. 14 for the unreinforced slab and in Fig. 15 for the reinforced slab.

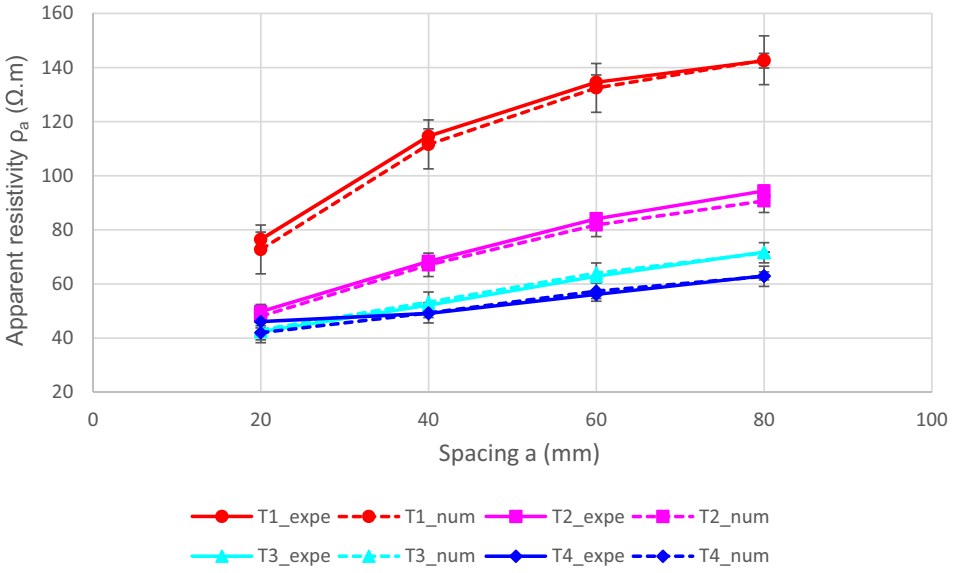

Fig. 14. Comparison of the experimental and numerical apparent resistivity values as a function of spacing for each test time for the unreinforced slab.

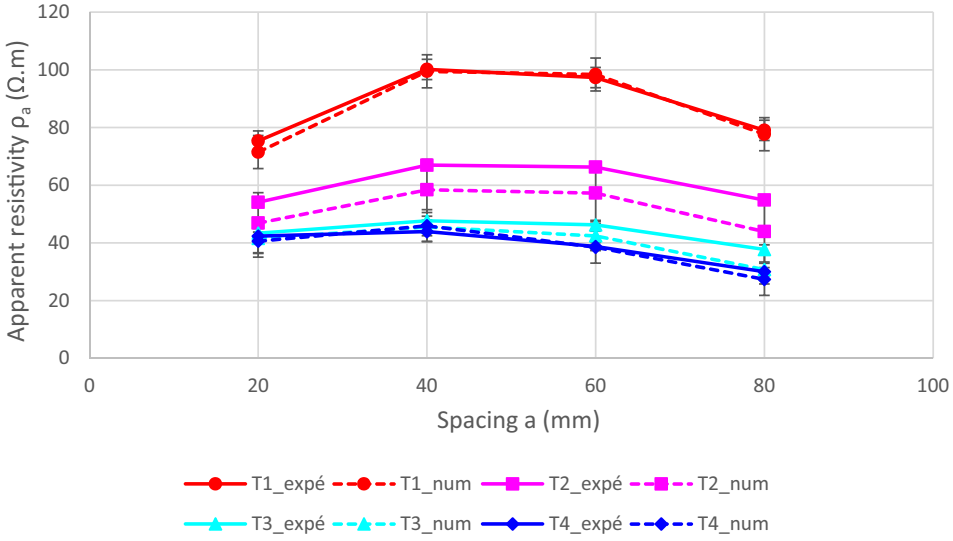

Fig. 15. Comparison of the experimental and numerical apparent resistivity values as a function of spacing for each test time for the reinforced slab.

For both the unreinforced and the reinforced synthetic models, the apparent resistivity values obtained by numerical analysis of the physical problem are in reasonable agreement with the experimental data (Figs. 13 and 14). Indeed, by calculating the normalized root-mean-square error (NRMSE) in percentage from the RMSE criterion (as defined in Eq. (5)), the NRMSE reaches low values (NRMSE = 4.5%) for the unreinforced case and stays around 33.6% for the reinforced one due to the slight differences in T2. This can be explained by the onsite testing conditions with a slight delay in the measurements between the two slabs.

4.6. Discussion

After comparing the experimental results to the ones carried out by numerical modeling, we find that the results are comparable for both slabs but in a more effective way in the unreinforced slab.

The differences may be due to uncertainties in the measurements. In fact, the standard deviation σ of the measurements is σ unreinforced = 3.33 and σ reinforced = 4.15. Moreover, the differences may derive from the change in the state of the material over time, or because of the difference between the slabs, or the arrangement of the reinforcement, or the approximation of the numerical solution, and in particular the simplifying form of the concrete resistivity gradient. The difference may be more visible with the reinforced slab, and that can be due to the higher uncertainties in the measurements.

The compatibility of numerical and experimental results leads to several observations. For both studied models, the finite element calculation has converged to a solution that is comparable to the real case study. In the studied case, this validates the numerical solution and asserts that it simulates the real physical problem to some reasonable extent.

Finally, based on the work hypotheses stated in Section 1, for the reinforced slab model, the comparison of the measured and simulated apparent resistivity values makes it possible to confirm that the presence of the reinforcements only disturbs the apparent resistivity and not the 'true' resistivity of the concrete, at least prior

to corrosion initiation. Indeed, the aim of solving the forward problem in applying to the concrete of the reinforced slab a resistivity profile obtained for the unreinforced reference slab is to approve that the actual state of the concrete in the initiation phase is not affected by the presence of reinforcement. It is conditioned by the presence of water and chlorides in this case. Steel reinforcements being much more conductive than the concrete slab, the electrical current takes the easiest way, which induces lower potential differences and leads to the decrease in the apparent resistivity measurements.

5. Conclusion

To conclude, this study aims to determine the effect of reinforcement on apparent resistivity measurements made on reinforced concrete structures. Indeed, the disruption of apparent resistivity measurements in the presence of reinforcement was clearly observed during the experimental campaign presented herein. In addition, these disturbances made it impossible to invert the measurements to obtain the 'true' resistivity distribution, preventing the interpretation of the results on these reinforced slabs.

In the preliminary study, the aim was to optimize the numerical model and methodology in order to study the influence of reinforcement. This study showed that the presence of reinforcement in a concrete structure induces a significant decrease in the apparent resistivity values for increasing electrode spacing. Then in the parametric study, characteristics related to the relative position of the steel bar and the measuring device have been varied in order to determine the sensitivity of the apparent resistivities to the presence of reinforcements as a function of these characteristics, and to validate the observation made previously. Thus, the study revealed that the effect of the reinforcement is all the more significant if the concrete cover is small, the measuring electrodes are close to the reinforcement or the spacing between electrodes is large. These trends could be expected, but it allowed the effects to be quantified. For instance, concerning the effect of the distance between the electrode line and the steel bar, in the case of one rebar and for an inter-electrode spacing of 40 mm, it is preferable to move the electrode line 80 mm away from the axis of the rebar so that the effect is less than 5%, for a concrete cover thickness of 30 mm.

Finally, the previous experimental data were presented in which apparent resistivity measurements were carried out on reinforced and unreinforced concrete slabs subjected to salt water imbibition. The numerical modeling of the unreinforced slab generates apparent resistivity values that are very similar to those measured experimentally, which validates the existence of a numerical solution that correctly approximates the physical problem without reinforcement. Moreover, assuming to have the same 'true' resistivity distribution in the concrete of the two slabs, reinforced and unreinforced, we find a numerical solution comparable to the results obtained experimentally by modeling the reinforced slab. This result makes it possible to argue that the reinforcements have an effect only on the apparent resistivity, and not on the 'true' resistivity of the concrete, and that the methodology developed in this work allows a good modeling of the effects observed.

For this, since the disturbances due to the presence of reinforcement are taken into account for the forward modelling of the apparent resistivity, some suggestions for further research can be made. An improvement of the apparent resistivity inversion method could make it possible to obtain the 'true' resistivity distribution despite the presence of reinforcements, provided that their characteristics are taken into consideration (position, geometry, electrical properties and contact with the concrete). Moreover, the study of the electrochemical effect of the steel and concrete interface, modeled by a Butler-Volmer type formulation, can take into account the effect of the reinforcement corrosion in modeling in order to represent more finely the reality and to obtain an even more reliable numerical solution.

Declaration of Competing Interest

None.

Acknowledgements

The authors would like to thank Région Pays de la Loire for their financial support, IFSTTAR and CEREMA for financing the experimental research project, Milia Fares (IFSTTAR), Benoit Thauvin and his team, especially Ronan Queguiner, (CEREMA, Laboratory of Saint Brieuc), for their contribution to the experimental campaign.

References

[1] M. Neville Adam, Properties of Concrete: Fourth and Final Edition, Pearson Education Limited, Harlow, England, 1995.
[2] AFPC-AFREM, Compte-rendu des journées techniques de l'AFPC-AFREM, Durabilité des Bétons, Méthodes recommandées pour la mesure des grandeurs associées à la durabilité, Toulouse, 1997.
[3] V. Baroghel-Bouny et al., Concrete Design for a given Structure Service Life – Durability Management with Regard to Reinforcement Corrosion and Alkali-Silica Reaction – State of the Art and Guid for the Implementation of a Predictive Performance Approach based upon Durability Indicators, Scientific and technical documents AFGC, 2007. English version.
[4] U.M. Angst, Predicting the time to corrosion initiation in reinforced concrete structures exposed to chlorides, Cem. Concr. Res. 115 (2019) 559–567.
[5] J.-P. Balayssac, V. Garnier, Non-destructive Testing and Evaluation of Civil Engineering Structures, Press Ltd & Elsevier Press Ltd., London, 2017.
[6] P. Gu, J. Beaudoin, Dielectric behavior of hardened cement paste systems, J. Mater. Sci. Lett. 15 (1996).
[7] M. Saleem, M. Shameemt, S. Hussain, M. Maslehuddintf, Effect of moisture, chloride and sulphate contamination on the electrical resistivity of Portland cement concrete, Constr. Build. Mater. 10 (1996) 209–214.
[8] M. Castellote, C. Andrade, C. Alonso, Measurement of the steady and non-steady-state chloride diffusion coefficients in a migration test by means of monitoring the conductivity in the anolyte chamber - Comparison with natural diffusion tests, Cem. Concr. Res. 3 (2001) 1411–1420.
[9] W. McCarter, M. Forde, H. Whittington, Resistivity characteristics of concrete, Proc. Inst. Civ. Eng. 71 (1981) 107–117.
[10] E. Hammond, T. Robson, Comparison of electrical properties of various cements and concretes, Eng 199 (1955) 78–80.
[11] J.F. Lataste, G. Villain, J.P. Balayssac, Chapter 4. Electrical Methods, in: Non-Destructive Test. Eval. Civ. Eng. Struct., ISTE Press Ltd & Elsevier Press Ltd., London, 2017.
[12] G. Monfore, The electrical resistivity of concrete, J. PCA Res. Dev. 10 (1968) 35–48.
[13] K. Pokkuluri, Effect of Admixtures, Chlorides, and Moisture on Dielectric Properties of Portland Cement Concrete in the Low Microwave Frequency Range, Faculty of the Virginia Polytechnic Institute and State University, 1998.
[14] E. Rasch, F. Hinrichsen, Uber eine Beziehung zwischen, Elektrischer Leitfahigkeit Und Temp, Z. Electrochem. 14 (1908) 41–48.
[15] G. Keller, F. Frischknecht, Electrical Methods in Geophysical Prospecting, Pergamon Press, Oxford, 1996.
[16] G. Villain, V. Garnier, M. Sbartaï, X. Dérobert, J.-P. Balayssac, Development of a calibration methodology to improve the on-site non-destructive evaluation of concrete durability indicators, Mater. Struct. (2018) 51–140.
[17] C. Andrade, C. Alonso, A. Arteaga, P. Tanner, Methodology Based on the Electrical Resistivity for the Calculation of Reinforcement Service Life, 5th Canmet/ACI Int. Conf. Durab. Concr., 2000, pp. 899–915.
[18] C. Andrade, R. D'Andréa, A. Castillo, M. Castel, The use of electrical resistivity as NDT method for the specification of the durability of reinforced concrete, Non-Destr. Test Civ. Eng. (2009).
[19] M. Chouteau, S. Beaulieu, An investigation on application of the electrical resistivity tomography method to concrete structures. in: 2nd Annu. Conf. Appl. Geophys. NDT Methodol. to Transp., 2002.
[20] W. Daily, A. Ramirez, A. Binley, D. LeBrecque, Electrical resistance tomography, Lead. Edge. 23 (2004) 438–442.
[21] K. Gowers, S. Millard, The effect of steel reinforcement bars on the measurement of concrete resistivity, Br. J. Non-Destruct Test. 33 (1991) 551–560.
[22] R. Polder, Test methods for on site measurement of resistivity of concrete- a RILEM TC-154 technical recommendation, Constr. Build. Mater. 15 (2001) 125–131.

[23] C. Andrade, R. Polder, M. Basheer, Non-destructive Evaluation of the Penetrability and Thickness of the Concrete Cover, in: Non-Destructive Methods to Meas. Ion Migr. RILEM RC 189-NEC State-of-the-Art Report., 2007.
[24] O. Sengul, O. Gjorv, Effect of embedded steel on electrical resistivity measurements on concrete structures, ACI Mater J. 106 (2009) 11–18.
[25] J. Wait, Geo-electromagnetism, London, 1982.
[26] A.Q. Nguyen, G. Klysz, F. Deby, J.P. Balayssac, Evaluation of water content gradient using a new configuration of linear array four-point probe for electrical resistivity measurement, Cem. Concr. Compos. 83 (2017) 308–322.
[27] A. Garzon, J. Sanchez, C. Andrade, N. Rebolledo, E. Menéndez, J. Fullea, Modification of four point method to measure the concrete electrical resistivity in presence of reinforcing bars, Cem. Concr. Compos. 83 (2014) 308–322.
[28] Y. Lim, T. Noguchi, C. Cho, Mathematical modeling for quantative estimation of geometric effects of nearby rebar in electrical resistivity measurement, Cem. Concr. Compos. 90 (2018) 82–88.
[29] M. Sohail, S. Laurens, F. Deby, J. Balayssac, Significance of macrocell corrosion of reinforcing steel in partially carbonated concrete: numerical and experimental investigation, Mater. Struct. 48 (2015) 217–233.
[30] A. Nasser, A. Clément, S. Laurens, A. Castel, Influence of steel–concrete interface condition on galvanic corrosion currents in carbonated concrete, Corros. Sci. 52 (2010).
[31] G. Samson, F. Deby, J.-L. Garciaz, J.-L. Perrin, A new methodology for concrete resistivity assessment using the instantaneous polarization response of its metal reinforcement framework, Constr. Build. Mater. 187 (2018) 531–544.
[32] F. Presuel-Moreno, Y. Liu, Y. Wu, Numerical modeling of the effects of rebar presence and/or multilayered concrete resistivity on the apparent resistivity measured via the Wenner method, Constr. Build. Mater. 48 (2013) 16–25.
[33] W. Telford, L. Geldart, R. Sheriff, Applied Geophysics, Cambridge University Press, Cambridge, 1990.
[34] H. Layssi, P. Ghods, A. Alizadeh, M. Salehi, Electrical resistivity of concrete, Concr. Int. 41–46 (2015).
[35] K. Gowers, S. Millard, Measurement of concrete resistivity for assessment of corrosion severity of steel using Wenner technique, ACI Mater. J. 96 (1999) 5.
[36] W. McCarter, G. Starrs, S. Kandasami, R. Jones, M. Chrisp, Electrode configurations for resistivity measurements on concrete, ACI Mater. J. 106 (2009) 258–264.
[37] W. McCarter, H. Taha, B. Suryanto, G. Starrs, Two-point concrete resistivity measurements: interfacial phenomena at the electrode–concrete contact zone, Meas. Sci. Technol. 26 (2015).
[38] F. Wenner, A method for measuring Earth resistivity, J. Washingt. Acad. Sci. 5 (1915) 561–563.
[39] R. Du Plooy, S. Lopes, G. Villain, X. Dérobert, Development of a multi-ring resistivity cell and multi-electrode resistivity probe for investigation of cover concrete condition, NDT&E Int. 54 (2013) 27–36.
[40] L. Marescot, S. Rigobert, S. Palma Lopes, R. Lagabrielle, D. Chapellier, A general approach for DC apparent resistivity evaluation on arbitrarily shaped 3D structures, J. Appl. Geophys. 60 (2006) 55–67.
[41] D. Demanet, E. Pirard, F. Renardy, D. Jongmans, Application and processing of geophysical images for mapping faults, Comput. Geosci. 27 (2001) 1031–1037.
[42] J. Lataste, M. Behloul, D. Breysse, Characterisation of fibres distribution in a steel fibre reinforced concrete with electrical resistivity measurements, NDT&E Int. 41 (2008) 638–648.
[43] A. Vickery, B. Hobbs, The effect of subsurface pipes on apparent resistivity measurements, Geophys. Prospect. 50 (2002) 1–13.
[44] M. Morales, Experimental, Investigation of the Effects of Embedded Rebar, Cracks, Chloride Ingress and Corrosion on Electrical Resistivity Measurements of Reinforced Concrete Master of Science thesis, State University, Oregon, 2015, p. 174.
[45] F. Presuel-Moreno et al., Characterization of New and Old Concrete Structures Using Surface Resistivity Measurements, Florida, Florida Department of Transportation Research Center, 2010, p. 279.
[46] J.M. Sanchez, Influence of Saturation and Geometry on Surface Electrical Resistivity Measurements Master of Applied Science Building Engineering thesis, Concordia University, Canada, 2015, p. 183.
[47] M. Castellote, C. Andrade, C. Alonso, Standardization, to a reference of 25 C, of the electrical resistivity values measured at any temperature for mortars and concrete in saturated conditions, ACI Mater. J. 99 (2) (2002) 119–128.
[48] Y. Liu, F. Presuel-Moreno, Normalization of temperature effect on concrete resistivity by method using Arrhenius Law, ACI Mater. J. 111 (4) (2014) 433–442.
[49] M. Loke, 1-D Resistivity, IP & SIP Inversion and forward modeling. Res1D ver. 1.00.09 Beta, (2001).
[50] M. Fares, Y. Fargier, G. Villain, X. Dérobert, S. Palma-Lopes, Determining the permittivity profile inside reinforced concrete using capacitive probes, NDT&E Int. 79 (2016) 150–161.